Research Article | Vol. 26, No. 14 | 9 Jul 2018 | OPTICS EXPRESS 18563
Optics EXPRESS

Deterministic generation of single soliton Kerr frequency comb in microresonators by a single shot pulsed trigger

ZHE KANG,[1,7] FENG LI,[1,2,7,8] JINHUI YUAN,[2,3,7,9] K. NAKKEERAN,[4] J. NATHAN KUTZ,[5] QIANG WU,[6] CHONGXIU YU,[3] AND P. K. A. WAI[1,2]

[1]*Photonics Research Centre, Department of Electronic and Information Engineering, The Hong Kong Polytechnic University, Hung Hom, Hong Kong*
[2]*The Hong Kong Polytechnic University Shenzhen Research Institute, 518057, Shenzhen, China*
[3]*State Key Laboratory of Information Photonics and Optical Communications, Beijing University of Posts and Telecommunications, 100876, Beijing, China*
[4]*School of Engineering, University of Aberdeen, Aberdeen, AB24 3UE, UK*
[5]*Department of Mathematics, University of Washington, Seattle, WA 98195, USA*
[6]*Department of Physics and Electrical Engineering, Northumbria University, Newcastle upon Tyne, NE1 8ST, UK*
[7]*These authors contributed equally*
[8]*lifeng.hk@gmail.com*
[9]*yuanjinhui81@bupt.edu.cn*

Abstract: Kerr soliton frequency comb generation in monolithic microresonators recently attracted great interests as it enables chip-scale few-cycle pulse generation at microwave rates with smooth octave-spanning spectra for self-referencing. Such versatile platform finds significant applications in dual-comb spectroscopy, low-noise optical frequency synthesis, coherent communication systems, etc. However, it still remains challenging to straightforwardly and deterministically generate and sustain the single-soliton state in microresonators. In this paper, we propose and theoretically demonstrate the excitation of single-soliton Kerr frequency comb by seeding the continuous-wave driven nonlinear microcavity with a pulsed trigger. Unlike the mostly adopted frequency tuning scheme reported so far, we show that an energetic single shot pulse can trigger the single-soliton state deterministically without experiencing any unstable or chaotic states. Neither the pump frequency nor the cavity resonance is required to be tuned. The generated mode-locked single-soliton Kerr comb is robust and insensitive to perturbations. Even when the thermal effect induced by the absorption of the intracavity light is taken into account, the proposed single pulse trigger approach remains valid without requiring any thermal compensation means.

© 2018 Optical Society of America under the terms of the OSA Open Access Publishing Agreement

OCIS codes: (190.4390) Nonlinear optics, integrated optics; (190.5530) Pulse propagation and temporal solitons; (140.3945) Microcavities.

References and links

1. D. J. Jones, S. A. Diddams, J. K. Ranka, A. Stentz, R. S. Windeler, J. L. Hall, and S. T. Cundiff, "Carrier-envelope phase control of femtosecond mode-locked lasers and direct optical frequency synthesis," Science **288**(5466), 635–640 (2000).
2. S. T. Cundiff and J. Ye, "Colloquium: Femtosecond optical frequency combs," Rev. Mod. Phys. **75**(1), 325–342 (2003).
3. A. Schliesser, N. Picqué, and T. W. Hänsch, "Mid-infrared frequency combs," Nat. Photonics **6**(7), 440–449 (2012).
4. J. Pfeifle, V. Brasch, M. Lauermann, Y. Yu, D. Wegner, T. Herr, K. Hartinger, P. Schindler, J. Li, D. Hillerkuss, R. Schmogrow, C. Weimann, R. Holzwarth, W. Freude, J. Leuthold, T. J. Kippenberg, and C. Koos, "Coherent terabit communications with microresonator Kerr frequency combs," Nat. Photonics **8**(5), 375–380 (2014).
5. K. Y. Yang, K. Beha, D. C. Cole, X. Yi, P. Del'Haye, H. Lee, J. Li, D. Y. Oh, S. A. Diddams, S. B. Papp, and K. J. Vahala, "Broadband dispersion-engineered microresonator on a chip," Nat. Photonics **10**(5), 316–320 (2016).

#326548 https://doi.org/10.1364/OE.26.018563
Journal © 2018 Received 20 Mar 2018; revised 4 Jun 2018; accepted 9 Jun 2018; published 5 Jul 2018

Optics EXPRESS

6. T. J. Kippenberg, R. Holzwarth, and S. A. Diddams, "Microresonator-based optical frequency combs," Science **332**(6029), 555–559 (2011).
7. T. Herr, K. Hartinger, J. Riemensberger, C. Wang, E. Gavartin, R. Holzwarth, M. Gorodetsky, and T. Kippenberg, "Universal formation dynamics and noise of Kerr-frequency combs in microresonators," Nat. Photonics **6**(7), 480–487 (2012).
8. S. B. Papp, K. Beha, P. Del'Haye, F. Quinlan, H. Lee, K. J. Vahala, and S. A. Diddams, "Microresonator frequency comb optical clock," Optica **1**(1), 10–14 (2014).
9. D. K. Armani, T. J. Kippenberg, S. M. Spillane, and K. J. Vahala, "Ultra-high-Q toroid microcavity on a chip," Nature **421**(6926), 925–928 (2003).
10. P. Del'Haye, A. Schliesser, O. Arcizet, T. Wilken, R. Holzwarth, and T. J. Kippenberg, "Optical frequency comb generation from a monolithic microresonator," Nature **450**(7173), 1214–1217 (2007).
11. D. J. Moss, R. Morandotti, A. L. Gaeta, and M. Lipson, "New CMOS-compatible platforms based on silicon nitride and Hydex for nonlinear optics," Nat. Photonics **7**(8), 597–607 (2013).
12. Y. Okawachi, K. Saha, J. S. Levy, Y. H. Wen, M. Lipson, and A. L. Gaeta, "Octave-spanning frequency comb generation in a silicon nitride chip," Opt. Lett. **36**(17), 3398–3400 (2011).
13. I. V. Barashenkov IV and Y. S. Smirnov, "Existence and stability chart for the ac-driven, damped nonlinear Schrödinger solitons," Phys. Rev. E Stat. Phys. Plasmas Fluids Relat. Interdiscip. Topics **54**(5), 5707–5725 (1996).
14. T. Herr, V. Brasch, J. Jost, C. Wang, N. Kondratiev, M. Gorodetsky, and T. Kippenberg, "Temporal solitons in optical microresonators," Nat. Photonics **8**(2), 145–152 (2014).
15. F. Leo, S. Coen, P. Kockaert, S.-P. Gorza, P. Emplit, and M. Haelterman, "Temporal cavity solitons in one-dimensional Kerr media as bits in an all-optical buffer," Nat. Photonics **4**(7), 471–476 (2010).
16. S. Coen, H. G. Randle, T. Sylvestre, and M. Erkintalo, "Modeling of octave-spanning Kerr frequency combs using a generalized mean-field Lugiato-Lefever model," Opt. Lett. **38**(1), 37–39 (2013).
17. M. R. Lamont, Y. Okawachi, and A. L. Gaeta, "Route to stabilized ultrabroadband microresonator-based frequency combs," Opt. Lett. **38**(18), 3478–3481 (2013).
18. H. Guo, M. Karpov, E. Lucas, A. Kordts, M. H. Pfeiffer, V. Brasch, G. Lihachev, V. E. Lobanov, M. Gorodetsky, and T. Kippenberg, "Universal dynamics and deterministic switching of dissipative Kerr solitons in optical microresonators," Nat. Phys. **13**(1), 94–102 (2017).
19. M. H. P. Pfeiffer, C. Herkommer, J. Q. Liu, H. R. Guo, M. Karpov, E. Lucas, M. Zervas, and T. J. Kippenberg, "Octave-spanning dissipative Kerr soliton frequency combs in Si_3N_4 microresonators," Optica **4**(7), 684–691 (2017).
20. X. Yi, Q.-F. Yang, K. Y. Yang, M.-G. Suh, and K. Vahala, "Soliton frequency comb at microwave rates in a high-Q silica microresonator," Optica **2**(12), 1078–1085 (2015).
21. X. Yi, Q. F. Yang, K. Youl Yang, and K. Vahala, "Active capture and stabilization of temporal solitons in microresonators," Opt. Lett. **41**(9), 2037–2040 (2016).
22. V. Brasch, M. Geiselmann, T. Herr, G. Lihachev, M. H. Pfeiffer, M. L. Gorodetsky, and T. J. Kippenberg, "Photonic chip-based optical frequency comb using soliton Cherenkov radiation," Science **351**(6271), 357–360 (2016).
23. J. A. Jaramillo-Villegas, X. Xue, P.-H. Wang, D. E. Leaird, and A. M. Weiner, "Deterministic single soliton generation and compression in microring resonators avoiding the chaotic region," Opt. Express **23**(8), 9618–9626 (2015).
24. V. E. Lobanov, G. V. Lihachev, N. G. Pavlov, A. V. Cherenkov, T. J. Kippenberg, and M. L. Gorodetsky, "Harmonization of chaos into a soliton in Kerr frequency combs," Opt. Express **24**(24), 27382–27394 (2016).
25. C. Joshi, J. K. Jang, K. Luke, X. Ji, S. A. Miller, A. Klenner, Y. Okawachi, M. Lipson, and A. L. Gaeta, "Thermally controlled comb generation and soliton modelocking in microresonators," Opt. Lett. **41**(11), 2565–2568 (2016).
26. A. Dutt, C. Joshi, X. Ji, J. Cardenas, Y. Okawachi, K. Luke, A. L. Gaeta, and M. Lipson, "On-chip dual-comb source for spectroscopy," Sci. Adv. **4**(3), e1701858 (2018).
27. Q. Li, T. C. Briles, D. A. Westly, T. E. Drake, J. R. Stone, B. R. Ilic, S. A. Diddams, S. B. Papp, and K. Srinivasan, "Stably accessing octave-spanning microresonator frequency combs in the soliton regime," Optica **4**(2), 193–203 (2017).
28. T. C. Briles, J. R. Stone, T. E. Drake, D. T. Spencer, C. Frederick, Q. Li, D. A. Westly, B. R. Illic, K. Srinivasan, S. A. Diddams, and S. B. Papp, "Kerr-microresonator solitons for accurate carrier-envelope-frequency stabilization." arXiv:1711.06251 (2017).
29. G. S. Mcdonald and W. J. Firth, "Switching dynamics of spatial solitary wave pixels," J. Opt. Soc. Am. B **10**(6), 1081–1089 (1993).
30. J. K. Jang, M. Erkintalo, S. Coen, and S. G. Murdoch, "Temporal tweezing of light through the trapping and manipulation of temporal cavity solitons," Nat. Commun. **6**(1), 7370 (2015).
31. H. Taheri, A. A. Eftekhar, K. Wiesenfeld, and A. Adibi, "Soliton formation in whispering-gallery-mode resonators via input phase modulation," IEEE Photonics J. **7**(2), 2200309 (2015).
32. J. K. Jang, M. Erkintalo, S. G. Murdoch, and S. Coen, "Writing and erasing of temporal cavity solitons by direct phase modulation of the cavity driving field," Opt. Lett. **40**(20), 4755–4758 (2015).
33. W. J. Firth and A. J. Scroggie, "Optical bullet holes: Robust controllable localized states of a nonlinear cavity," Phys. Rev. Lett. **76**(10), 1623–1626 (1996).

Optics EXPRESS

34. S. Barland, J. R. Tredicce, M. Brambilla, L. A. Lugiato, S. Balle, M. Giudici, T. Maggipinto, L. Spinelli, G. Tissoni, T. Knödl, M. Miller, and R. Jäger, "Cavity solitons as pixels in semiconductor microcavities," Nature **419**(6908), 699–702 (2002).
35. J. K. Jang, M. Erkintalo, S. G. Murdoch, and S. Coen, "Ultraweak long-range interactions of solitons observed over astronomical distances," Nat. Photonics **7**(8), 657–663 (2013).
36. F. Leo, L. Gelens, P. Emplit, M. Haelterman, and S. Coen, "Dynamics of one-dimensional Kerr cavity solitons," Opt. Express **21**(7), 9180–9191 (2013).
37. E. Obrzud, S. Lecomte, and T. Herr, "Temporal solitons in microresonators driven by optical pulses," Nat. Photonics **11**(9), 600–607 (2017).
38. M. Haelterman, S. Trillo, and S. Wabnitz, "Dissipative modulation instability in a nonlinear dispersive ring cavity," Opt. Commun. **91**(5-6), 401–407 (1992).
39. F. Li, J. H. Yuan, Z. Kang, Q. Li, and P. K. A. Wai, "Modeling Frequency Comb Sources," Nanophotonics **5**(2), 292–315 (2016).
40. T. Hansson and S. Wabnitz, "Frequency comb generation beyond the Lugiato–Lefever equation: multi-stability and super cavity solitons," J. Opt. Soc. Am. B **32**(7), 1259–1266 (2015).
41. T. Hansson, D. Modotto, and S. Wabnitz, "Mid-infrared soliton and Raman frequency comb generation in silicon microrings," Opt. Lett. **39**(23), 6747–6750 (2014).
42. T. Carmon, L. Yang, and K. Vahala, "Dynamical thermal behavior and thermal self-stability of microcavities," Opt. Express **12**(20), 4742–4750 (2004).
43. K. Padmaraju and K. Bergman, "Resolving the thermal challenges for silicon microring resonator devices," Nanophotonics **3**(4–5), 269–281 (2014).
44. X. Xue, Y. Xuan, C. Wang, P.-H. Wang, Y. Liu, B. Niu, D. E. Leaird, M. Qi, and A. M. Weiner, "Thermal tuning of Kerr frequency combs in silicon nitride microring resonators," Opt. Express **24**(1), 687–698 (2016).
45. C. Bao, Y. Xuan, J. A. Jaramillo-Villegas, D. E. Leaird, M. Qi, and A. M. Weiner, "Direct soliton generation in microresonators," Opt. Lett. **42**(13), 2519–2522 (2017).
46. C. Bao, A. Weiner, Y. Xuan, D. Leaird, and M. Qi, "Directly stabilized solitons in silicon-nitride microresonators," in CLEO: Science and Innovations (Optical Society of America, 2017), p. SM2I. 1.
47. C. Bao, J. A. Jaramillo-Villegas, Y. Xuan, D. E. Leaird, M. Qi, and A. M. Weiner, "Observation of fermi-pasta-ulam recurrence induced by breather solitons in an optical microresonator," Phys. Rev. Lett. **117**(16), 163901 (2016).
48. M. Yu, J. K. Jang, Y. Okawachi, A. G. Griffith, K. Luke, S. A. Miller, X. Ji, M. Lipson, and A. L. Gaeta, "Breather soliton dynamics in microresonators," Nat. Commun. **8**, 14569 (2017).

1. Introduction

Since the use of self-referencing technique to stabilize carrier-envelope phase (CEP) was demonstrated in 2000 [1], optical frequency combs lead to revolutionary breakthrough in many fields such as spectroscopy, metrology, communications, biochemical sensing, etc [2–4]. Kerr frequency combs, as a branch of the frequency comb family, can be generated through modulation instability (MI) and cascaded four-wave mixing (FWM) in externally driven nonlinear microresonators [5–7]. Microresonators, typically structured as disk [5,8], toroid [9,10], or ring [11,12], have the advantages of compactness, high finesse, and CMOS compatibility. Externally driven microresonators are intrinsically driven-damped nonlinear systems, which normally exhibit multistable and chaotic dynamics depending on the system parameters [13]. Such dynamical behaviors have been observed in the experiments of microresonator-based Kerr frequency comb formation [14]. Temporal dissipative cavity solitons are first demonstrated in fiber cavity [15], which are stable solitons superimposed on a continuous-wave (CW) background, can be achieved through comb formation. Especially, the single cavity soliton (SCS) state shows many attractive characteristics, e.g. the generation of few-cycle femtosecond pulses at microwave rates and octave spanning phase-locked comb spectra [14,16,17]. However, straightforward and deterministic generation of the desired single-soliton state remains a challenge. The typical approach to obtain the single-soliton Kerr combs is to tune the pump frequency across a resonant frequency of the cavity from blue-detuned side to effectively red-detuned side [10,14]. Various improvements to the basic pump tuning scheme have been proposed and demonstrated. They include experimental demonstrations such as the combined forward and backward pump tuning to successively reduce the number of solitons generated in the microresonator [18,19] and a two-step "power kicking" protocol to overcome the thermal destabilization [20–22], and theoretical works like a specified tuning pathway obtained by prior scanning of the parameter space to achieve the

Optics EXPRESS

deterministic SCS by avoiding the chaotic and unstable states [23] and slow pump tuning in conjunction with phase or amplitude modulation [24]. However, any pump tuning scheme requires tunable lasers which in general suffer from broad linewidth and thus high noise density and degrade the frequency/phase noise characteristics of the combs. Tuning the cavity resonance by current-controlling a resistive heater has been proposed to excite single-soliton with fixed-frequency pump lasers [25,26]. Although these tuning based approaches show promising performances, it would be more attractive to straightforwardly and deterministically generate the SCS state without any tuning and active servo control. Furthermore, SCS generation schemes that minimize the thermal effect are particularly important for microresonators with fast thermal response. For instance, the thermal response time of silicon nitride (SiN) microresonators can be as short as hundreds of nanoseconds [27,28]. The tuning speed of most lasers or microheaters cannot match such a fast thermally-induced cavity resonance shift, making it difficult for frequency-tuning based schemes to generate SCS. Phase modulation of the pump field has been proposed to deterministically excite the SCS instead of the tuning approaches [29–32]. However, the roundtrip times of Group IV (Si, SiN) and Group III-V (AlN) semiconductors based microresonators are typically in the order of a few picoseconds. Currently there are no commercially available phase modulators that could achieve such high-speed operation.

In this paper, we propose to generate single-soliton Kerr combs by seeding the CW pumped microcavity with a single shot pulsed trigger. The proposed method does not require any frequency tuning process, thus the complication induced by the fast thermal response issue is largely avoided. Also in the proposed triggering scheme, as will be discussed later, the cavity starts from the red-detuned side of the cold cavity and evolves into the SCS state along the nearest path, thus avoiding the chaotic states. As the extra energy injected into the microresonator is small, the variation of intracavity energy is kept at a low level. Consequently, the thermal effect induced resonant frequency shift of the microresonator is much smaller than that of the frequency tuning schemes. Similar cavity soliton excitation schemes by using addressing pulse have been proposed in spatial structures [33,34] and fiber cavities [15,35,36]. However, in microresonators the cavity roundtrip time is typically either comparable to or even shorter than the duration of the trigger pulse. Thus the full trigger pulse is likely to cover multiple cavity roundtrip time. The coherent stacking of the trigger pulse may cause destructive perturbation to the intracavity field. Furthermore, the thermal effects will not be a problem in the large volume fiber or spatial cavities. A recent work shows deterministic generation of SCS in a Fabry–Pérot microresonator by using synchronous pulsed pump instead of the common CW pump [37]. Although such a scheme can tolerate a small amount of non-synchronization, it cannot be used in microresonators with picosecond roundtrip time because it is difficult to obtain several hundreds of GHz pulse sources. More important, the pulsed pump must always be kept on because it serves as the pump, not a trigger. It is difficult to keep the pulse train synchronized to the cavity for a long period of time. Thus, the proposed trigger approach to generate SCS in microresonators is novel and unique.

2. Principles and methods

Figure 1(a) illustrates the proposed Kerr comb generation scheme. The combined field of a CW pump and a trigger pulse is injected into the microring resonator. The trigger pulse injects energy to those comb lines within the resonant profiles of the cavity and simultaneously covered by the spectrum of the trigger pulse. Most importantly, the phases of the comb lines are intrinsically synchronized as they are generated from the same single pulse trigger. Such coherently seeded comb lines initiate the Kerr comb generation process and avoid the random build-up of pulses through modulation instability (MI). Figure 1(b) shows a schematic diagram of the relationship between the spectral profiles of a trigger pulse train and the microresonator modes for three pulse periods T. When a single trigger pulse, i.e. $T = \infty$

Optics EXPRESS

(Case (iii)) is used, the pulse spectrum has the most off-resonant components, thus the least efficient energy coupling from the trigger pulse to the microresonator. However, the spectrum of the trigger pulse will certainly overlap with the resonant modes of the cavity. Thus, problems such as synchronization, timing jitter, and carrier envelope phase (CEP) stabilization will not arise if a single pulse is used as a trigger (Case (iii)), but are inevitable if a pulse train is used as trigger instead (Cases (i) and (ii)). In practice, any low repetition rate picosecond or femtosecond lasers with sufficient peak power and single pulse energy to excite an SCS can be used to construct the single shot trigger pulse source. The trigger pulse source is simply switched off after launching a single pulse into the cavity.

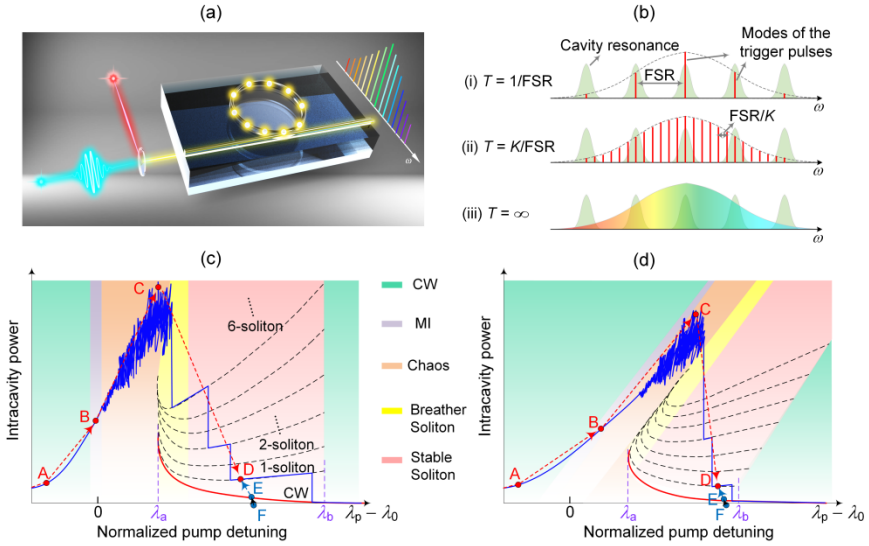

Fig. 1. (a) Schematic diagram of the proposed single-soliton Kerr comb generation. (b) Schematic diagram of the spectral profiles of a trigger pulse train at three different pulse period T (i) T = 1/FSR, where FSR is the free spectral range of the microresonator, (ii) $T = K$/FSR, where K is a positive integer, and (iii) $T = \infty$ (single shot trigger pulse). (c) and (d) are the illustrative diagrams of the variation of averaged intracavity power versus pump-resonance detuning in the Kerr comb excitation process when (c) only Kerr effect, and (d) both Kerr and thermal effects are considered. The blue solid curves show the possible intracavity power evolution to approach a single-soliton state in conventional pump frequency tuning scheme. The black dashed curves indicate the states with different number of intracavity solitons [14,18]. The lower red solid curve indicates the stable cold state with CW field only in the cavity. The evolution path to the single-soliton state utilizing the pump frequency tuning scheme (A→B→C→D) and the proposed trigger scheme (F→E→D) are indicated by the red and blue dashed arrows, respectively. Different colored regions indicate different intracavity states. MI stands for modulation instability. λ_p is the pump wavelength, and λ_0 is the closest cold-cavity resonant wavelength. λ_a and λ_b mark the wavelength detuning region where the SCS state exists as indicated in (c) and (d).

The wavelength of the CW pump is fixed and red-detuned [$\lambda_a < (\lambda_p - \lambda_0) < \lambda_b$] with respect to the closest cold-cavity resonant wavelength (λ_0), where λ_p is the pump wavelength, λ_a and λ_b mark the wavelength detuning range that SCS state exists, as indicated in Figs. 1(c) and 1(d). The evolution path to the SCS state in the proposed trigger scheme is rather different from that of the conventional pump tuning scheme. The schematic diagrams in Figs. 1(c) and 1(d) show the variation of the average intracavity power versus the pump-resonance detuning, which have terraced soliton solution states (black dashed curves). Kerr effect is included in both figures but thermal effect is considered in Fig. 1(d) only [14,18]. From Figs. 1(c) and 1(d), as the pump wavelength is increased from the blue-detuned side to the effectively red-detuned side, the cavity undergoes the (A) CW, (B) MI, (C) chaotic which is also called unstable MI, and (D) SCS state along the path A→B→C→D. In the proposed trigger scheme,

Optics EXPRESS

the cavity starts from (F) cold state in the red-detuned side, first jumps to (E) a stable cold equilibrium CW state, and then to (D) the SCS state along the path F→E→D, by the combined action of the CW and trigger pulse. The inclusion of thermal effect tilts the response curve, as shown in Fig. 1(d), but the dominant behaviors shown in Figs. 1(c) and 1(d) are similar.

We note that the intracavity power of the SCS state (D) is much lower than that of the chaotic state (C). To reach the SCS state from the chaotic state, the cavity will have to be significantly cooled down. The excess energy should be quickly shed, otherwise the SCS state cannot be accessed and sustained. The difficulty to dissipate the excess energy is the reason that the resonance is typically lost when the pump wavelength enters the effectively red-detuned region in conventional pump tuning experiments. Thus special tuning speed control, power kicking methods, and/or active servo control, which are equivalent to thermal annealing of the microcavity, are required to obtain and stabilize the SCS state from the chaotic state [14,20–22]. Despite the use of these special means, conventional pump tuning scheme to reach the SCS state remains unpredictable because it starts from a chaotic state. In the proposed trigger scheme, as the microcavity will not go through any chaotic state, the final state is deterministic. As the variation of intracavity energy is much smaller than that of the pump tuning scheme, the proposed trigger scheme is more robust to thermal perturbations.

Since the trigger field is the combination of a CW pump and a pulse, the light injected into the resonator is not a fixed quantity but varies significantly. Thus for the proposed trigger scheme, the mean-field Lugiato-Lefever equation (LLE) is no longer adequate to describe the system. We model the evolution of the optical field inside the cavity using the Ikeda map [38–40],

$$\psi^{(m+1)}(z=0,\tau)=\sqrt{\theta}\psi_{\mathrm{in}}^{(m)}(\tau)+\sqrt{1-\theta}e^{-i\delta_0}\psi^{(m)}(z=L,\tau), \tag{1}$$

$$\frac{\partial\psi^{(m)}(z,\tau)}{\partial z}=-\frac{\alpha_0}{2}\psi^{(m)}+i\sum_{k\geq 2}\frac{i^k\beta_k}{k!}\frac{\partial^k\psi^{(m)}}{\partial\tau^k}+i\gamma\left(1+i\tau_{\mathrm{s}}\frac{\partial}{\partial\tau}\right)\left|\psi^{(m)}\right|^2\psi^{(m)}. \tag{2}$$

where $\psi^{(\mathrm{m})}(z,\tau)$ is the slowly-varying envelope of the intracavity optical field in the m-th roundtrip, τ is the retarded time, α_0 is the linear loss coefficient, θ is the coupling coefficient between the microring and the bus waveguide, β_{k} is the k-th order dispersion coefficient, γ is the nonlinear coefficient, $L = 2\pi r$ is the roundtrip length, r is the radius of the resonator, $\delta_0 = t_{\mathrm{R}}(\omega_0 - \omega_{\mathrm{p}}) = 2\pi l - \phi_0$ is the detuning between the CW pump frequency ω_{p} and its closest l-th order cold-cavity resonant frequency ω_0, here t_{R} is the roundtrip time of the resonator and l is an integer, ϕ_0 is the linear phase delay of the intracavity field in a single roundtrip, and $\tau_{\mathrm{s}} = 1/\omega_{\mathrm{p}}$ is the optical shock time constant. The dispersion of the nonlinearity is typically negligible for the reported microresonators [8–12,14,18,20–22,41], but can be included by referring to the modeling of supercontinuum generation [39] for specific materials and operation bands. The combined injection signal of a CW pump and a single shot pulse during the m-th roundtrip is given by,

$$\psi_{\mathrm{in}}^{(m)}(\tau)=\psi_{\mathrm{cw}}+\sqrt{P_{\mathrm{t}}}\exp\left[-i\Delta\Omega(\tau+mt_{\mathrm{R}})\right]\mathrm{sech}\left[(\tau+mt_{\mathrm{R}}-\delta t)/\tau_{\mathrm{t}}\right]. \tag{3}$$

where ψ_{cw} is the CW pump field, P_{t} and τ_{t} represent the peak power and duration of the trigger pulse, respectively. δt represents the temporal central position of the trigger pulse. $\Delta\Omega = 2\pi\Delta f = 2\pi(f_{\mathrm{t}} - f_{\mathrm{cw}})$ is the central frequency offset of the trigger with respect to the CW pump, where f_{t} and f_{cw} are the central frequencies of the trigger pulse and the CW field, respectively. The fast variation of the combined injection field is completely described by Eq. (3). We note that phase matching between the trigger pulse and the roundtrip phase of the CW pump is not required. Different phases difference only result in different interference profiles of the combined optical fields of the trigger pulse and the CW pump, but does not prevent the excitation of the SCS.

Optics EXPRESS

Thermal effects become significant only after the formation of the SCS but contribute little during the initial transient Kerr process. Therefore, we first study the trigger approach on SCS generation without including the thermal effect in Eqs. (1) and (2). The thermal effect is discussed and studied individually.

3. Results and discussion

3.1 SCS excitation with a single shot pulse trigger

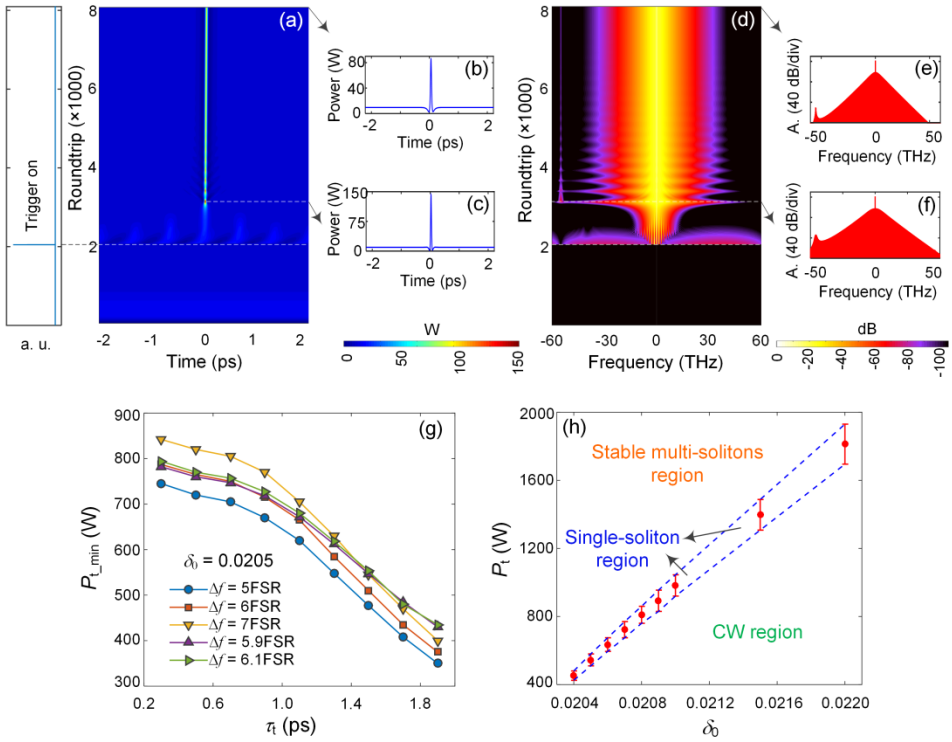

Fig. 2. (a)-(c) Temporal and (d)-(f) spectral evolutions of the intracavity field and the instantaneous profiles at the final and 3084-th roundtrips, respectively, when a single shot pulse trigger with a peak power of 520 W and an FWHM of 1.5 ps is injected. (g) P_{t_min} versus τ_t at different Δf. (h) Different operation regions within the parameter space of P_t and δ_0 with τ_t = 1.5 ps and Δf = 6·FSR. Other parameters: $|\psi_{cw}|^2$ = 1 W, β_2 = –59 ps^2/km, γ = 1 W^{-1}/m, $\alpha_0 L$ = 0.012. Dispersion parameters up to 7-th order are included to properly describe the broadband dispersion characteristics of the resonator.

To demonstrate the effectiveness of the proposed trigger approach, we use a Si_3N_4 microring resonator fabricated on silicon oxide substrate as an example, which is similar to that reported in [12,17]. We also note that Eqs. (1)-(3) can be applied to microresonators fabricated by other materials. The resonator has a free spectral range (FSR) of 226 GHz, a radius of r = 100 μm, and a coupling coefficient between the bus and ring waveguides of θ = 0.25%. The loaded Q-factor is ~1 × 10^5. The detuning δ_0 is fixed to 0.0205 here. A single shot pulse with a peak power of 520 W is launched at the 2050-th roundtrip, accompanying the CW pump of 1 W, as shown in the inset of Fig. 2(a). The power might be doubled in practice as a beam splitter is likely required to combine the two optical fields. After the injection of the trigger pulse, the peaks of the interference profiles between the trigger pulse and the CW pump first evolve into several weak pulses. Eventually the central one, which has the highest peak power, evolves into a stable SCS. No chaotic or MI states are experienced. Figure 2(b) shows the intracavity temporal waveform at the final roundtrip of the simulation. The SCS has a

Optics EXPRESS

peak power of 86 W and FWHM of 43.4 fs. The waveform at the 3084-th roundtrip is shown in Fig. 2(c), which is captured at the first peak of a damped oscillation in the evolution. The cavity soliton has a higher peak power of 143 W and a smaller FWHM of 32 fs when compared with the final state. Figures 2(d), 2(e), and 2(f) show the spectral evolution, spectral profiles of the intracavity field at the final and the 3084-th roundtrips, respectively. Figure 2(d) shows that an initial broadband gain is introduced by the high energy single shot pulse trigger, which initiates and accelerates the generation of the Kerr comb lines.

Figure 2(g) shows the minimum P_t required for SCS generation versus the pulse width τ_t for different central frequency offset Δf. The required P_{t_min} decreases when τ_t increases. For the Δf values which are integer multiples of the FSR, a larger Δf corresponds to a larger P_{t_min}. The relationship is reasonable since larger Δf will reduce the period of the beating oscillation caused by the interference between the trigger pulse and CW pump, which reduces the energy within each interfered peak. The reduction of energy has to be compensated at the expense of increasing P_{t_min}. When Δf deviates slightly from an integer multiple of the FSR, e.g. Δf = 5.9·FSR and 6.1·FSR, P_{t_min} deviates from the original curve especially when τ_t is larger than 1 ps. For such Δf, the roundtrip time will no longer be an integer multiple of the oscillation period, which may lead to destructive interference because of the coherent stacking of different parts of the pulse that leaked into adjacent roundtrips. Such perturbation will become significant when the trigger pulse is relatively long. For example, with a trigger pulse width of 1.5 ps, a Δf deviation of ± 0.1·FSR from 6·FSR will increase the power threshold by ~40 W. For the same deviation of Δf, the power penalty is only ~5 W if the trigger pulse width is 0.5 ps only. With a 0.5 ps pulse, the SCS state can be excited even when Δf is decreased from 6.0·FSR to 5.5·FSR, i.e. the central frequency of the pulse locates at the middle of two resonances of the microcavity, with a fixed peak power equal to P_{t_min} at Δf = 6.0·FSR. Thus, with an ultrashort trigger pulse whose spectra can cover several FSR, the SCS excitation is insensitive to the central frequency offset of the trigger pulse. In Fig. 2(g), the P_{t_min} curves of Δf = 5.9·FSR and 6.1·FSR begin to deviate from that of Δf = 6.0·FSR when τ_t is about 1 ps. Thus, the best choice of the trigger pulse width should be <1 ps for the configuration of the microresonator under studied. Figure 2(h) shows the different working regions in the parameter space (P_t, δ_0) at τ_t = 1.5 ps and Δf = 6·FSR. For the δ_0 considered, there is always a band of P_t bounded by the two blue dashed curves that ensures SCS generation. The region above this band lead to stable multi-solitons states, while only CW states can be found in the region below this band. The details in Figs. 2(g) and 2(h) will be changed when thermal effect is included, but the basic trend and characteristics remain the same.

3.2 Deterministic SCS excitation

SCS excitation using the conventional frequency tuning approach is not deterministic because the intracavity field must undergo the chaotic state before the SCS state can be reached [14,23]. We compare the conventional pump frequency tuning approach with the proposed single shot pulse trigger approach by introducing temporal perturbations to the CW field of the conventional tuning approach, and both the CW field and the trigger pulse of the proposed trigger approach. The perturbation is defined as $\sigma = \eta\tilde{N}\exp(i2\pi\tilde{U})$. Here $\tilde{N}$ is a normally distributed random variable with zero mean value and standard deviation of 1, $\tilde{U}$ is a uniformly distributed random variable between 0 and 1, and $\eta = 1 \times 10^{-8}$ is the factor denoting the amplitude of the perturbation. The other parameters used in the pump tuning case are the same as those in Fig. 2 except for the varied δ_0.

Optics EXPRESS

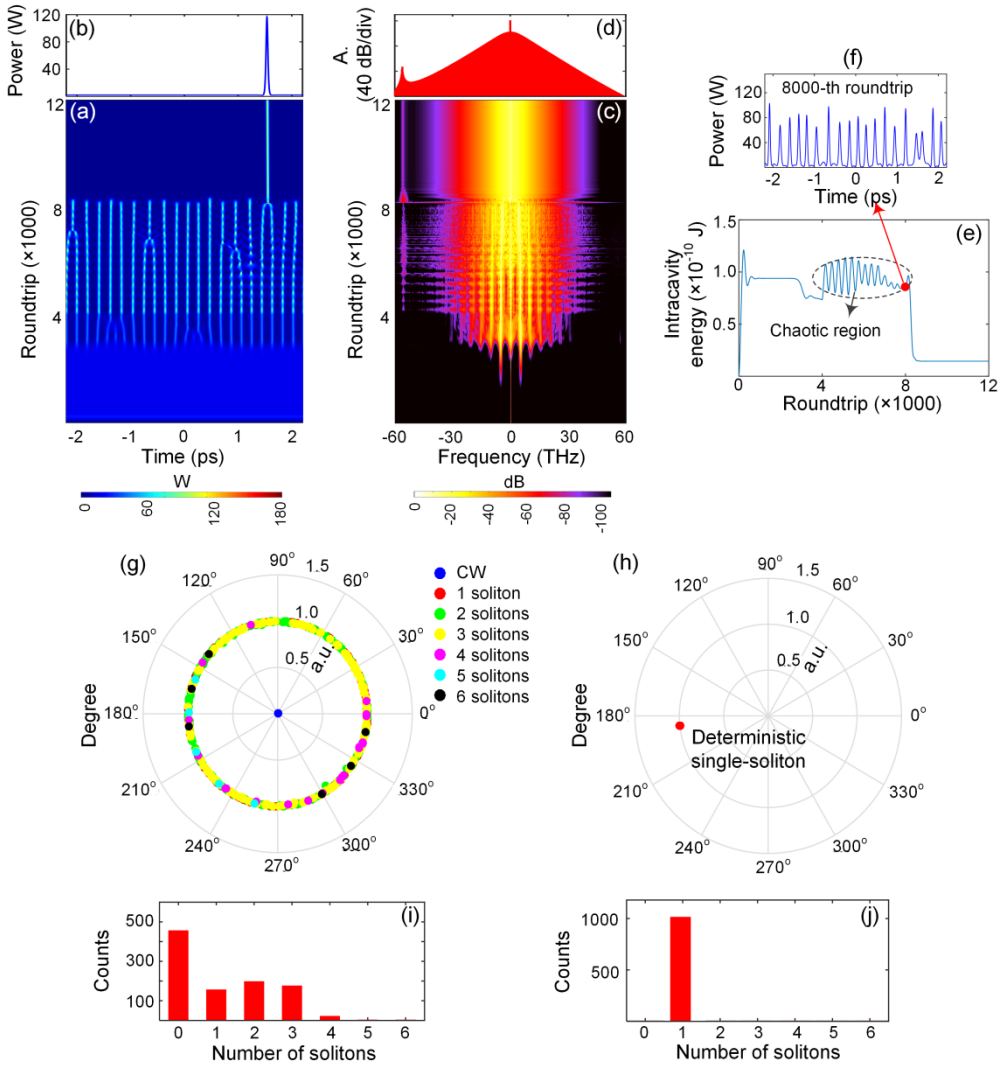

Fig. 3. (a)-(b) Temporal and (c)-(d) spectral evolutions of the intracavity field and the instantaneous profiles at the final roundtrip. (e) The intracavity energy at each roundtrip. (f) Instantaneous temporal profile at the 8000-th roundtrip of the pump frequency tuning approach. 1,000 simulation results using (g) the pump frequency tuning and (h) the proposed trigger approaches, respectively. The counts of different soliton states of the 1,000 simulations using (i) the pump frequency tuning and (j) the trigger approaches, respectively.

Figures 3(a) and 3(c) respectively show the temporal and spectral evolutions of the cavity field using the pump frequency tuning approach. Figures 3(b) and 3(d) show the instantaneous temporal and spectral profiles of the cavity field at the final roundtrip (12,000-th) of the simulation, respectively. δ_0 is initially set to –0.005, and increased to 0.018 and 0.035 at the 4000-th and 8000-th roundtrips, respectively. MI and chaotic states of the intracavity field are observed before the excitation of SCS. Multi-soliton states could also be excited if δ_0 is chosen to a value between 0.018 and 0.035 at 8000-th roundtrip. Figure 3(e) shows the evolution of the intracavity energy during the dynamics. The chaotic region is clearly indicated by the large oscillations of the energy. Figure 3(f) shows the instantaneous temporal profile at the 8000-th roundtrip, which presents a group of pulses with random-like locations and amplitudes in the chaotic state. The results of 1,000 simulations for the pump

Optics EXPRESS

frequency tuning and trigger approaches are shown in Figs. 3(g) and 3(h), respectively. The temporal positions and peak power of the solitons are plotted as the azimuthal angle and radial position in polar coordinates. The temporal positions in the range of $[-t_R/2, t_R/2]$ are mapped into azimuthal angles in [0°, 360°], corresponding to the positions in the microring. The angular positions of all intracavity solitons are recorded despite of the final state. The peak power is normalized to the maximum peak power of the single-soliton case. It is clear that the final soliton states are not deterministic. The number of intracavity solitons varies from zero to six. Even CW states are observed. In contrast, the proposed trigger approach always deterministically excites the cavity to the SCS state despite the perturbations, as shown in Fig. 3(h). Figures 3(i) and 3(j) show the counts of different soliton states with the pump tuning and trigger approaches, respectively. It is surprising that CW state without any intracavity soliton is the mostly observed state with the pump frequency tuning approach. The count of single-soliton with the pump frequency tuning approach is only 154 out of 1,000, while single soliton state is obtained in all of the 1,000 simulations with the proposed trigger approach.

3.3 Thermally self-stabilized SCS

Compared with large volume fibers or spatial cavities, the thermal effect is much stronger for nanoscale microcavities [42]. The dissipated energy heats up the microcavities and induces changes in the refractive indices. Thus, the resonant frequencies of the cavities are shifted by the thermo-optic effect and the pump-resonance detuning cannot be modeled as a fixed value any more. The development of athermal optical materials and advanced cooling techniques are promising in overcoming the thermal problem, but up to now, these techniques still cannot fully avoid the thermal effect in microcavities [43].

The thermal effect leads to the thermal instability of the effectively red-detuned region [42], which forces the frequency scanning to start from the blue-detuned side in conventional pump tuning schemes. Thermal instability of the red-detuned region is the phenomenon that a pump initially injected at the near red-detuned side of a microresonator eventually operates in the effectively blue-detuned side because of the thermal effect. From Fig. 1(d), if the pump at λ_p is initially injected at the red-detuned region $0 < (\lambda_p - \lambda_0) < \lambda_a$ of a cold microresonator, the combined thermal and Kerr effects will push the microcavity to operate in one of the states (CW or MI) on the blue solid curve above, which is in the effectively blue-detuned side [14,18,42]. If the pump starts the frequency scanning from a wavelength detuning $(\lambda_p - \lambda_0) > \lambda_a$, the microcavity will stay at a cold CW state represented by the lower red solid curve in Fig. 1(d). As the cold CW state is very stable and has a lower intracavity power, it cannot reach the soliton states with higher intracavity power unless additional energy is injected into the microcavity. Scanning the pump frequency from the red-detuned region towards the blue-detuned side will eventually run into the thermal instability (when $(\lambda_p - \lambda_0) < \lambda_a$) and will not arrive at any of the soliton states.

In the proposed trigger scheme, the CW pump wavelength λ_p is not tuned but fixed to a value in the region $\lambda_a < (\lambda_p - \lambda_0) < \lambda_b$ at a cold microresonator state (point F). Thus the thermal instability of red-detuned region is avoided. The microresonator will therefore first operate in the stable cold CW state (point E) and then get pushed up to the SCS state (point D) by the trigger pulse. We will show that the energy variation of this transition is small which only results in a small thermal shift, thus does not destroy the SCS state. We include the thermal effect into the model and divide the temporal triggering procedure of the SCS states into two stages, i.e. the CW and CS stages. In the CW stage, only the CW pump accumulates in the cavity and reaches the thermally stabilized state. Along the intracavity power accumulation, the resonant frequency of the cavity gets red-shifted towards the pump frequency, thus the pump-resonance detuning is reduced. Then, in the CS stage, the single shot trigger pulse is injected to excite the SCS state. If the thermally shifted pump-resonance detuning at the end of the CW stage still locates in the detuning region that supports CSs, then the SCS can be

Optics EXPRESS

excited by the trigger pulse in the early CS stage. The thermal effect does not affect the initial excitation of SCS because the thermal response time of Si_3N_4 waveguide is typically microseconds or sub-microseconds [44,45], which is much longer than the excitation time of CS (~1000 roundtrips, 4 ns). The thermally shifted detuning is very small in such short transient time. However, the increase of intracavity energy due to the injected pulse trigger does further shift the cavity resonant frequency, which might annihilate the excited SCS after thermal relaxation.

We first study the thermal effect in the CW stage. Since the intracavity CW field does not vary significantly between consecutive roundtrips and considering the extremely long thermal stabilization process, we use a modified LLE to improve the computation efficiency,

$$t_R \frac{\partial \psi}{\partial t} = \sqrt{\theta}\psi_{in} - \frac{\alpha_0 L + \theta}{2}\psi - i(\delta_0 + \delta_{therm})\psi + iL\sum_{k\geq 2}\frac{i^k \beta_k}{k!}\frac{\partial^k \psi}{\partial \tau^k} + i\gamma L(1 + i\tau_s \frac{\partial}{\partial \tau})|\psi|^2 \psi, \quad (4)$$

$$\frac{d\delta_{therm}}{dt} = -\frac{\delta_{therm}}{\tau_0} + \frac{\xi}{t_R}\int_0^{t_R} |\psi|^2 \, d\tau. \quad (5)$$

where $\delta_{therm} = t_R(\omega_{therm} - \omega_0)$ is the thermally induced detuning shift, ω_{therm} is the thermally shifted cavity resonant frequency. τ_0 is the thermal response time determined by the material of the microresonator and the thermal dissipation in experiments. ξ is the coefficient representing the detuning shift in response to the average intracavity power. We use τ_0 = 100 ns and $\xi = -4.5 \times 10^4$ $W^{-1}s^{-1}$ in the simulation according to a practically fabricated high-Q (~1.1×10^6) Si_3N_4 microresonator [45,46], which has comparable volume and parameters to the one used in Fig. 2 except a smaller propagation loss of $\alpha_0 L = 0.0012$. Comparing with the thermo-optic effect of Si_3N_4, the contribution of thermal expansion effect is much smaller and can be neglected [44,45]. Hence, $\xi \propto \wp C \alpha_0 L$ depends on the thermo-optic coefficient $\wp$ of Si_3N_4, the heat capacity C of the microring, and the ratio that intracavity power is absorbed and converted to heat. We can use the ξ value at $\alpha_0 L = 0.0012$ as a reference to calculate ξ at other loss parameters.

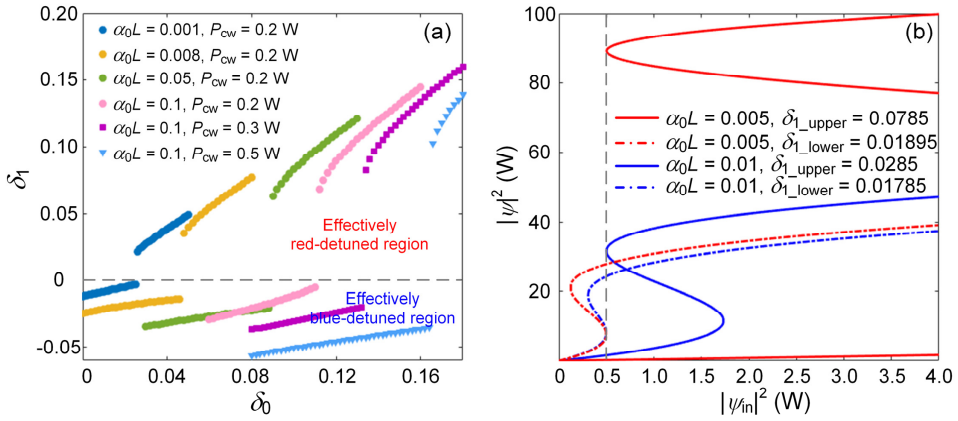

Fig. 4. (a) Stabilized δ_1 at the end of CW stage starting from a cold cavity as a function of initial detuning δ_0 under different propagation loss and pump power. Other parameters: γ = 1.4 W^{-1}/m, L = 628 μm, θ = 0.0025, t_R = 4.425 ps. (b) S-curves with the border detuning values δ_{1_lower} and δ_{1_upper} for the pump power of 0.5 W when $\alpha_0 L$ are 0.005 and 0.01, respectively.

Figure 4(a) shows the stabilized detuning $\delta_1 \equiv \delta_0 + \delta_{therm}$ at the end of CW stage versus initial detuning δ_0 under different propagation loss and pump power. Simulation is carried out for 5×10^6 roundtrips (~22 μs) to guarantee thermal stabilization in the CW stage. We find that, for a given pump power and loss, there is a lowest initial detuning δ_{0_min} to ensure that

Optics EXPRESS

the shifted detuning will still remain within the red-detuned side. The final stabilized detuning δ_1 will be positive (effectively red-detuned) only if $\delta_0 \geq \delta_{0\_min}$, which is a necessary condition for CS excitation. When $\delta_0 < \delta_{0\_min}$, δ_1 becomes negative (effectively blue-detuned), thus no CS can be excited. The results are consistent with that shown in [42], which indicates two kinds of thermal equilibriums, i.e. stable warm equilibrium (effectively blue-detuned) and stable cold equilibrium (effectively red-detuned) CW states can be reached. With the increase of propagation loss, the threshold δ_{0_min} also increases since more intracavity power is converted to heat. δ_{0_min} will also increase when the pump power P_{cw} increases. The detuning value δ_{0_min} gives the critical value to reach an effectively red-detuned state, which corresponds to the lowest red solid curve in Fig. 1(d).

It is known that the CS states exist almost in the same bistable region of the stationary CW solution solved by Ikeda map or LLE [15,40]. The two models give the same bistable region when the nonlinear length is much longer than the cavity length [16,40]. Since the thermal effect responds in a long time scale, we can focus on the initial stage of the CS stage and obtain the stationary CW solution by setting the derivative terms in Eq. (4) to zeros and neglecting the variation of δ_1 in the transient triggering process. The equation becomes

$$Y = \frac{\gamma^2 L^2}{\theta} X^3 - \frac{2\delta_1 \gamma L}{\theta} X^2 + \frac{(\delta_1^2 + \alpha^2)}{\theta} X. \tag{6}$$

where $Y = |\psi_{in}|^2$ is the pump power, $X = |\psi|^2$ is the intracavity power, $\alpha = (\alpha_0 L + \theta)/2$ is the total loss per roundtrip. The turning points of the function $Y(X)$ can be calculated by setting the first derivative dY/dX to zero as

$$3\gamma^2 L^2 X^2 - 4\delta_1 \gamma L X + (\delta_1^2 + \alpha^2) = 0. \tag{7}$$

The function $X(Y)$ given by Eq. (6) has a bistable region when Eq. (7) has two different real roots of X, which requires $\delta_1^2 > 3\alpha^2$. The two real roots corresponding to the two turning points of the bistable curve are given by

$$X_{1,2} = \frac{2\delta_1 \pm \sqrt{\delta_1^2 - 3\alpha^2}}{3\gamma L}. \tag{8}$$

Substituting these roots into Eq. (6), we obtain the minimum and maximum of P_{cw} in the bistable region for given values of δ_1 and α. By sweeping the values of δ_1, the limited bistable regions are found in the 2-dimensional (P_{cw}, δ_1) space with $\alpha_0 L$ values varying from 0.0012 to 0.012, shown in Fig. 5 as the green regions confined by the two orange boundary curves in each map. The two specific loss values, i.e. $\alpha_0 L$ = 0.0012 and 0.012, correspond to two practically fabricated Si_3N_4 microresonators [12,17,45,46]. The other two loss values of $\alpha_0 L$ = 0.004 and 0.008 are arbitrarily chosen between the two specific values. In each green bistable region, there are two boundary detuning values δ_{1_upper} and δ_{1_lower} of δ_1 for each P_{cw}. In the detuning range of $\delta_{1\_lower} < \delta_1 < \delta_{1\_upper}$ with a given pump power P_{cw}, the system always has two stable solutions. Figure 4(b) shows two sets of S-curves with the boundary detuning values δ_{1_lower} and δ_{1_upper} for a pump power P_{cw} = 0.5 W. When the loss $\alpha_0 L$ is 0.005, the δ_{1_upper} (red solid curve) and δ_{1_lower} (red dashed curve) are calculated to be 0.0785 and 0.01895, respectively. The difference between δ_{1_upper} and δ_{1_lower} is 0.0595. When $\alpha_0 L$ is increased to 0.01, δ_{1_upper} = 0.0285 (blue solid curve) and δ_{1_lower} = 0.01785 (blue dashed curve) are obtained. Compared to that of $\alpha_0 L$ = 0.005, the difference between δ_{1_upper} and δ_{1_lower} is reduced to 0.0107, which means the range of valid δ_1 becomes narrower. The trend of the variation agrees with that of the green regions in Fig. 5.

If the thermally-stabilized detuning δ_1 falls into the region bounded by δ_{1_upper} and δ_{1_lower} at the end of the CW stage, SCS can be excited very quickly after the injection of the single shot trigger pulse. Figure 5 shows the minimum possible values of δ_1 (blue dots) that can be stabilized in the red-detuned side with their fitting (blue dashed curves). In experiments, the

Optics EXPRESS

combinations of P_{cw} and corresponding δ_1 above the blue curves can be obtained by referring to the results in Fig. 4(a). Thus we can easily identify the valid regions (hatched regions in Fig. 5) for SCS excitation when thermal effect is taken into account, which are the overlapping area of the green and required δ_1 regions. When the loss $\alpha_0 L$ is increased, i.e. the Q-factor of the microresonator is decreased, Figs. 5(a)-5(d) show that the region bounded by δ_{1_upper} and δ_{1_lower} becomes narrower. Meanwhile, the required minimum pump power P_{cw} and minimum detuning δ_1 in the hatched region are both increased. Since injecting a CW light with several watts of power into a nanoscale waveguide is not practical, it is hard to excite the SCS in low-Q Si_3N_4 microresonators under the influence of thermal effect. The threshold of the Q-factor defined as "low-Q" depends on the operating range of the pump power. For the given pump power ranging from 0 to 1.2 W, Fig. 5(d) shows that there is no valid region for a cavity with $\alpha_0 L = 0.012$ (Q-factor ~1×10^5). In contrast, when $\alpha_0 L$ is 0.0012 (Q-factor ~1.1×10^6), Fig. 5(a) shows that the hatched region is quite large, which means the selection of initial δ_0 becomes very flexible.

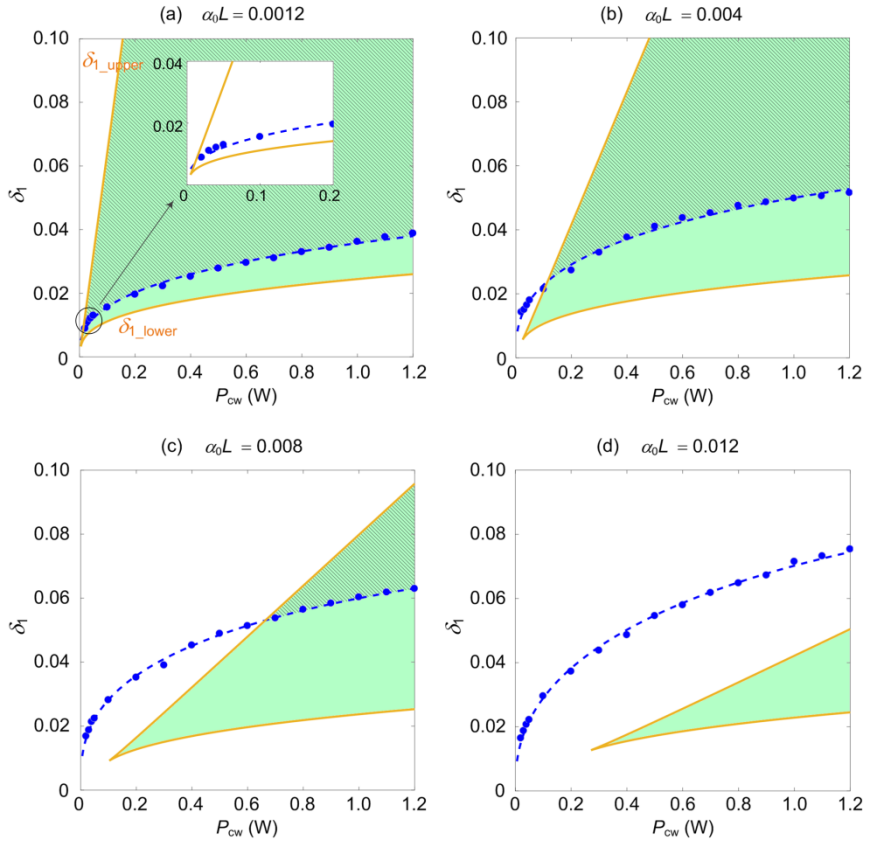

Fig. 5. The green regions are the possible CS excitation regions (bistable regions) bounded by the detuning δ_{1_upper} and δ_{1_lower}. Blue dashed curves with dots show the minimum δ_1 that can be thermally stabilized in the red-detuned side. Hatched regions indicate the valid regions for SCS excitation with thermal effect. The loss $\alpha_0 L$ is (a) 0.0012, (b) 0.004, (c) 0.008, and (d) 0.012, respectively. The inset in (a) shows the zoom-in view of the pump power ranging from 0 to 0.2 W.

From Fig. 5(a), we arbitrarily choose a pump power value of $P_{cw} = 0.03$ W and an initial detuning of $\delta_0 = 0.018$ which corresponds to a δ_1 value within the hatched region, and simulate both the CW and CS stages with the inclusion of thermo-optics effect. Considering both the coherent stacking of the leaked pulse tails of the full trigger pulse and the fast

Optics EXPRESS

variation of the intracavity field between consecutive roundtrips, we simulate the SCS triggering process in the CS stage using a modified Ikeda map, which is similar to that of Eqs. (1)-(3) except that we replace δ_0 by $\delta_0 + \delta_{therm}$ and add the thermal dynamics governed by Eq. (5). We also assume that the variation of δ_{therm} is small in one roundtrip and update the δ_{therm} value in steps of t_R.

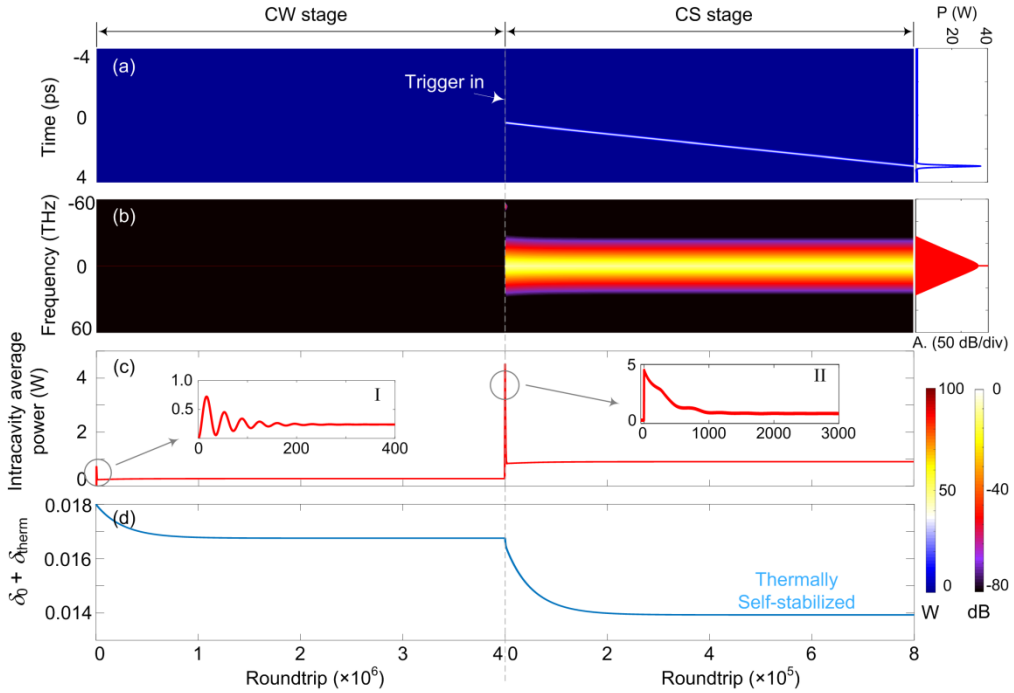

Fig. 6. (a) Temporal evolution and final instantaneous temporal profiles (b) spectral evolution and final instantaneous spectral profiles in the CW and CS stages. (c) Evolution of intracavity average power. Inset I and II show the zoom-in views in [0, 400] roundtrips of the CW stage and [0, 3000] roundtrips of the CS stage, respectively. (d) Evolution of $\delta_0 + \delta_{therm}$.

Figures 6(a) and 6(b) show the intracavity temporal and spectral evolutions along with the instantaneous temporal and spectral profiles at the end of the CS stage, respectively. The corresponding variations of intracavity average power and $\delta_0 + \delta_{therm}$ are shown in Figs. 6(c) and 6(d), respectively. The intracavity average power experiences a relaxation oscillation in the initial several hundreds of roundtrips (inset I of Fig. 6(c)), then increases slowly in the long thermal stabilization process and eventually converges to a fixed power of 0.2772 W. The detuning $\delta_0 + \delta_{therm}$ varies significantly in the first 1×10^6 roundtrips of the CW stage and slowly converges to 0.016753. The complete thermal stabilization of the cavity is achieved after ~2×10^6 roundtrips. A single shot 0.5 ps hyperbolic secant pulse with a peak power of 7.5 kW is launched at the end of CW stage to initiate the CS stage. The SCS is excited in ~1000 roundtrips (4.42 ns), and more importantly the newly excited SCS survives and is thermally self-stabilized in the subsequent evolution. The average power and $\delta_0 + \delta_{therm}$ are stabilized to 0.90375 W and 0.013933, respectively, in ~6×10^5 roundtrips of the CS stage. The stability of the SCS under thermal perturbation is the main advantage of the proposed pulse trigger approach. Unlike the conventional frequency tuning method, in which the tuning process is typically at microseconds level (comparable to or even longer than the thermal response time) and the intracavity field typically experiences the higher energy chaotic states, the SCS can be directly excited within several nanoseconds without going through any chaotic dynamics in the proposed pulse trigger approach. Hence, the thermal perturbation during the SCS excitation process is negligible as heating is a slow process. In the subsequent

Optics EXPRESS

evolution at the thermal response time scale, the variation of the intracavity energy caused by the trigger pulse will further affect the detuning until the thermal equilibrium is reached. Since the energy variation is small, the transition from the CW state to the SCS state only results in a small thermal shift, which will not destroy the excited soliton state. We find that the final detuning $\delta_0 + \delta_{therm} = 0.013933$ is still in the green region and larger than the boundary value $\delta_{1\_lower} = 0.0073$. Thus, the SCS will not be annihilated, but slowly adjust the working point with respect to the gradually changed detuning by thermal effect, and eventually gets thermally self-stabilized. It should be pointed out that it is not recommended to excite the SCS with δ_1 close to the lower boundary δ_{1_lower}, where breather CS states may appear [18,47,48]. The energy of the breather CSs is continually changing so that it is hard to be thermally self-stabilized. The exact thermally self-stabilization region of the SCS is not given in this paper, but will be studied in future work. However, we expect that this region will become broader for high-Q microresonators since the optical energy converted to heat is less, and the CSs valid region bounded by δ_{1_upper} and δ_{1_lower} will become broader too.

4. Conclusions

In conclusion, we propose to directly and deterministically generate single-soliton Kerr comb in a continuous-wave pumped microring resonator by seeding it with a pulsed trigger. Single cavity soliton can be straightforwardly and deterministically triggered by an energetic single shot pule without going through any multi-stable or chaotic states in the nonlinear microcavity. The feasibility of single shot trigger approach makes it possible to manipulate the number of solitons and their temporal locations inside the cavity by simply controlling the power and temporal location of the single pulse trigger. The proposed trigger approach can be applied to different type of microresonators as long as the microresonators do support cavity solitons. Moreover, we find that even under strong thermal effect the proposed trigger approach is valid to excite single cavity solitons in practically fabricated Si_3N_4 microresonators. No additional complex engineering is required for thermal compensation. Benefiting from the fast triggering process and relatively slow thermal dynamics caused by the intracavity optical heating, single cavity solitons can be easily excited within a broad parameters range and thermally self-stabilized in long-term evolutions. Since the triggering process is insensitive to the central frequency offset of the single shot trigger pulse when the pulse width is much shorter than the roundtrip time, the choice of trigger source is very flexible and feasible. The thermally self-stabilized single cavity solitons suggested that the proposed trigger approach can be applied to microresonators fabricated by current fabrication foundries to generate deterministic cavity solitons, which will pave the way to many applications of single-soliton Kerr combs.

Funding

Hong Kong Research Grants Council (PolyU152471/16E); The Hong Kong Polytechnic University (1-ZVGB); National Natural Science Foundation of China (NSFC) (61307109, 61475023, and 61475131); Shenzhen Science and Technology Innovation Commission (JCYJ20160331141313917); Beijing Youth Top-notch Talent Support Program (2015000026833ZK08).

139.133.148.27 {ts '2018-07-17 07:08:17'}